Astron. Astrophys. 152, 121–129 (1985)

ASTRONOMY AND ASTROPHYSICS

Magnetic stellar winds: a 2-D generalization of the Weber-Davis model

T. Sakurai *

Max-Planck-Institut für Physik und Astrophysik, Karl-Schwarzschild-Strasse 1, D-8046 Garching, Federal Republic of Germany

Received February 18, accepted April 29, 1985

Summary. A numerical method is presented to calculate steady, axisymmetric wind models with frozen-in magnetic fields. As a straightforward generalization of the model of Weber and Davis (1967), the wind solution along the magnetic field is obtained by an algebraic Bernoulli equation for the density. There appear two critical points, the slow mode and the fast mode critical points. The shape of the poloidal magnetic field should be determined by requiring the balance of force across the field line. This leads to the second order partial differential equation for the magnetic stream function. This equation is singular at the Alfvén surface and the regularity condition there together with the inner boundary condition uniquely determines the solution. Examples of computations were carried out by adopting a monopole-like basic configuration. The important feature found in the numerical solution is the poleward deflection of the wind flow due to the magnetic force of spiraling field lines. Asymptotic behavior of the solution at large distances shows that the flow does not become radial but is collimated in the direction of the rotation axis. There arises a dense polar column around the rotation axis, in which the magnetic pinching force is balanced by the pressure of the confined gas.

Key words: stellar winds – solar wind – hydromagnetics

1. Introduction

The braking of stellar rotation due to stellar winds has been proposed (Schatzman, 1962) to account for a transition along the main sequence from rapid to slow rotators around the spectral type F5. That is, the surface convection zone of the late type stars provides both the magnetic field (due to a dynamo) and the hot corona (also due to some magnetic mechanism). And the wind with the magnetic field exerts a braking torque, which is much larger than expected for non-magnetic winds, by increasing the effective length of the torque arm.

The first quantitative theory of magnetic stellar winds was developed by Weber and Davis (1967). Their model deals with the steady, polytropic, axisymmetric flow of an inviscid and perfectly conducting fluid. The geometry of their model is monopole-like (a "split-monopole" model), i.e. the poloidal magnetic field is radial and is oppositely directed above and below the equatorial plane. This configuration therefore possesses an equatorial current sheet with a high gas pressure to balance the magnetic forces. This feature is not essential mathematically, however, as far as the current sheet is approximated by an infinitely thin layer. Weber and Davis (1967) solved the problem near the equator and evaluated the time scale of the spin down of the Sun to be $\simeq 7\ 10^9$ yr (provided the angular momentum is mixed uniformly within the Sun).

The model by Weber and Davis (1967) has three "critical points" where the flow velocity matches the wave velocity of three magnetohydrodynamic (MHD) wave modes (slow mode, fast mode, and Alfvén mode, respectively). This situation is more complicated than in the case of non-magnetic winds (Parker, 1958), which has one critical point corresponding to sonic waves. The approach which Weber and Davis (1967) used is applicable equally to the region outside of the equator (Yeh, 1976). But in any case the model does not consider the force-balance perpendicular to the poloidal magnetic field. (The poloidal field is assumed instead.) Therefore the model is one-dimensional (1-D) and one only needs to solve the model along each flux tube independently.

On the other hand if one tries to assure the force-balance across the poloidal field and to determine the field structure self-consistently, one ends up with a second order partial differential equation in two spatial coordinates in the poloidal plane (i.e. 2-*D* modelling). An attempt to solve this problem was made by Pneuman and Kopp (1971), Mestel (1968), and by Okamoto (1974, 1975). The iterative method used by Pneuman and Kopp (1971) is to solve alternatively the wind equation along the field and the force-balance equation across the field. Okamoto (1975), however, claimed that the equation for the latter process has a singularity which was not considered by Pneuman and Kopp (1971) and cast doubt on their computation (this point will be discussed in detail in Sect. 4). In a series of papers Mestel (1961, 1967, 1968) and Okamoto (1974, 1975) presented the analytical formulation of the problem but they did not give a detailed numerical treatment comparable to that of Pneumann and Kopp (1971). In addition one might be sceptical about their analysis because they did not pay attention to the fast mode critical point.

In this paper we will present a method which solves the 2-*D* wind model numerically. The method is a natural extention of the 1-*D* Weber-Davis model, and in Sect. 2 we will first summarize the

* On leave of absence from Department of Astronomy, University of Tokyo, Tokyo 113, Japan

basic characteristics of the Weber-Davis model briefly. Some of them are basically the review of previous works (Weber and Davis, 1967; Yeh, 1976), but some new results will also be presented. Especially an efficient procedure to find the wind solution along the magnetic field is introduced, which is made use of in the method described in Sect. 3 to solve the 2-*D* problem. In Sect. 3 an example of a 2-*D* computation will be presented, which shows that the flow tends to be collimated in the direction of the rotation axis. This behavior will also be explained by studying the asymptotic solution at large distances. In the light of these results, in Sect. 4 the present method will be compared to that of Pneuman and Kopp (1971).

One feature which complicates the analysis in extending 1-*D* models to 2-*D* is the appearance of the dead zone (a closed field region with no outflow). The ratio of the magnetic fluxes in the dead zone and the wind zone was shown to be an important factor in determining the spin-down rate of the star (Mestel, 1968). The present analysis adopts a monopole geometry as the basic configuration, however, mainly because of the mathematical and numerical complexity in treating both the wind and the dead zones. Due to this simplifying assumption, a direct comparison between the Weber-Davis model and corresponding 2-*D* models is possible. A model including the dead zone will be developed in a future paper. We should keep in mind, however, that in addition to mathematical/numerical difficulties, the existence of the dead zone will also introduce physical complications such as the possible instability of the discontinuity between the two zones.

2. 1-D model of Weber and Davis (1967)

2.1. *Definition of the model*

This model is described by six equations for six variables, density ϱ, pressure p, radial and azimuthal components of the velocity and the magnetic field, V_r, V_φ, B_r, and B_φ. We use spherical polar coordinates (r, θ, φ) and solves the problem near the equator $\theta = \pi/2$. Equations which determine the model are

$$p = K\varrho^\gamma, \tag{1}$$

$$\varrho V_r r^2 = f, \tag{2}$$

$$B_r r^2 = \Phi, \tag{3}$$

$$(V_\varphi - \Omega r) B_r = V_r B_\varphi, \tag{4}$$

$$r\left(V_\varphi - \frac{B_r B_\varphi}{4\pi\varrho V_r}\right) = \Omega r_A^2, \tag{5}$$

$$\frac{V_r^2}{2} + \frac{1}{2}(V_\varphi - \Omega r)^2 + \frac{\gamma}{\gamma-1}\frac{p}{\varrho} - \frac{GM}{r} - \frac{\Omega^2 r^2}{2} = E. \tag{6}$$

M is the mass of the star and G is the gravitational constant. Six integration constants K, f, Φ, Ω, r_A, and E have been introduced. Equation (1) is the polytropic relation with polytropic index γ (=const). Equations (2) and (3) are respectively the conservation of mass and magnetic fluxes. Equation (4) is equivalent to the frozen – in condition expressed in the form that the flow velocity and the magnetic field are parallel to each other in the coordinate frame rotating with the angular velocity Ω. Equation (5) is the conservation of angular momentum. Equation (6) is the Bernoulli integral of the equation of motion in the rotating frame, with the centrifugal potential $-\Omega^2 r^2/2$. Since the magnetic force has no component in the direction of the flow in the rotating frame, (6) has no magnetic term. Weber and Davis (1967) used the Bernoulli integral defined in the rest frame, in which $V_\varphi - \Omega r$ is replaced by V_φ and a Poynting flux term appears instead of the centrifugal term $-\Omega^2 r^2/2$. Their energy constant is different from E in (6) by a constant $\Omega^2 r_A^2/2$.

These six equations determine the solution after the values of the six parameters K, f, Φ, Ω, r_A, and E are given. Usually Ω is taken as the rotation rate of the central star into which the field lines are anchored. In addition at the base of the corona $r = r_*$, the values of density ϱ_*, pressure p_*, and the field strength B_{r*} can be specified. Therefore two more conditions are necessary to fix the solution. In the following it will be shown that the existence of two critical points supplies these two conditions.

If (1)–(5) are substituted into (6), the equation that only involves the density ϱ is obtained. This is the Bernoulli equation which determines the density profile $\varrho(r)$, namely,

$$H(r, \varrho) = E, \tag{7}$$

where

$$H(r, \varrho) = \frac{GM}{r_A}\tilde{H}(x, y), \tag{8}$$

$$x = r/r_A, \quad y = \varrho/\varrho_A, \quad \varrho_A = 4\pi f^2/\Phi^2, \tag{9}$$

$$\tilde{H}(x, y) = \frac{\beta}{2x^4 y^2} + \frac{\Theta}{\gamma-1} y^{\gamma-1} - \frac{1}{x} + \frac{\omega}{2}\left\{\frac{(x-1/x)^2}{(y-1)^2} - x^2\right\}, \tag{10}$$

and

$$\beta = \frac{\Phi^2}{4\pi GM\varrho_A r_A^3} = \left[V_{Ar}^2 \Big/ \frac{GM}{r}\right]_A, \tag{11a}$$

$$\Theta = \frac{\gamma K \varrho_A^{\gamma-1} r_A}{GM} = \left[C_S^2 \Big/ \frac{GM}{r}\right]_A, \tag{11b}$$

$$\omega = \frac{\Omega^2 r_A^3}{GM} = \left[\Omega^2 r^2 \Big/ \frac{GM}{r}\right]_A. \tag{11c}$$

Here $C_S^2 = \gamma p/\varrho$ is the sound speed squared and $V_{Ar}^2 = B_r^2/4\pi\varrho$ is the radial Alfvén speed squared. The subscript A stands for the Alfvén point, because $(\varrho/\varrho_A)^{-1/2} = V_r/V_{Ar}$ is the Alfvén Mach number which is unity if $\varrho = \varrho_A$.

Essential points of the model are summarized as follows.

1. The density profile $\varrho(r)$ is a level contour of the Bernoulli function $H(r, \varrho)$ in the (r, ϱ)-plane.

2. At $\varrho = \varrho_A$, $H(r, \varrho)$ diverges if $r \neq r_A$ but remains finite if $r = r_A$. That is, $\varrho = \varrho_A$ is an infinitely high wall in the (r, ϱ)-space with a hole at (r_A, ϱ_A). Therefore all the solutions which go from sub-Alfvénic $(\varrho > \varrho_A)$ to super-Alfvénic $(\varrho < \varrho_A)$ regions automatically pass through the Alfvén point (r_A, ϱ_A) in the (r, ϱ)- plane.

3. An X-type critical point (or O-type point) of the level contour $\varrho(r)$ arises where the function $H(r, \varrho)$ is locally flat, i.e.

$$\frac{\partial H}{\partial \varrho} = \frac{\partial H}{\partial r} = 0. \tag{12}$$

4. The curve $\partial H/\partial\varrho = 0$ in the (r, ϱ)-plane will be called the slow/fast mode Mach curve, by observing

$$\begin{aligned}\varrho\frac{\partial H}{\partial \varrho} &= -V_r^2 - \frac{\Omega^2\varrho}{\varrho - 4\pi f^2/\Phi^2}\left(\frac{V_r B_\varphi}{B_r}\right)^2 + K\varrho^{\gamma-1} \\ &= -\frac{V_r^4 - V_r^2(C_S^2 + V_{Ar}^2 + V_{A\varphi}^2) + C_S^2 V_{Ar}^2}{V_r^2 - V_{Ar}^2} \\ &= -\frac{(V_r^2 - V_{sr}^2)(V_r^2 - V_{fr}^2)}{V_r^2 - V_{Ar}^2}\end{aligned} \tag{13}$$

($V_{A\varphi}^2 = B_\varphi^2/4\pi\varrho$). Therefore $\partial H/\partial\varrho$ vanishes where V_r equals either the slow mode velocity V_{sr} or the fast mode velocity V_{fr}.

5. The curve $\partial H/\partial r = 0$ in the (r, ϱ)-plane will be called the gravitational throat curve. In regarding the transonic wind as the flow through de Laval nozzle (Parker, 1963), the throat of the nozzle is located at $\partial H/\partial r = 0$.

6. The intersection of the slow (fast) Mach curve and the gravitational throat curve gives the slow mode critical point (r_s, ϱ_s) [the fast mode critical point (r_f, ϱ_f)], respectively. Therefore two conditions are imposed there, i.e.

$$H(r_s, \varrho_s) = E,$$
$$H(r_f, \varrho_f) = E. \tag{14}$$

Thus the wind solution will be uniquely determined.

Figure 1a and b show a typical layout of Mach curves, throat curves, and the solution curves. The relevant wind solution which starts with a slow ($V_r < V_{sr}$) velocity at small r and attains a high velocity ($V_r > V_{fr}$) at large r is shown by the thick curve. The Alfvén point is a focus of a bundle of solutions and plays no role in selecting a particular solution. Rigorously speaking, it should be referred to as *the Alfvén point* and *not* as the Alfvén critical point. As we will see in Sect. 3, however, *the Alfvén critical point* appears as the singularity in the cross-field force-balance equation. This is understandable because the Bernoulli equation is an equation for the density, and the Alfvén wave, without density perturbation, will not show up in it.

2.2. *Classification of wind models by dimensionless parameters*

Some of the wind solutions thus obtained are similar to each other except for the difference in scaling. To see this point, we will rewrite (7) in a dimensionless form

$$\tilde{H}(x, y; \beta, \Theta, \omega) = \tilde{E}. \tag{15}$$

$\tilde{E}$ is a constant which substitutes $E[\tilde{E} = E/(GM/r_A)]$. The wind solution is obtained by requiring

$$\frac{\partial\tilde{H}}{\partial x} = \frac{\partial\tilde{H}}{\partial y} = 0, \quad \tilde{H} = \tilde{E},$$
$$\text{at} \quad (x, y) = (x_s, y_s) \quad \text{and} \quad (x_f, y_f), \tag{16}$$

where subscripts s and f refer respectively to slow and fast mode critical points. Among the eight variables (x_s, x_f, y_s, y_f, β, Θ, ω, and $\tilde{E}$), six are determined by these equations if the remaining two are specified. If for example the values of Θ and ω are specified, the variables x_s, x_f, y_s, y_f, $\tilde{E}$, and β are determined as functions of Θ and ω. Therefore any wind solution is characterized by two dimensionless parameters Θ and ω, which respectively measure the strength of thermal pressure and centrifugal force in accelerating the wind. The reason why we use these and not the third parameter which measures the effect of magnetic field [β in (11a)] is that the magnetic force alone cannot accelerate the wind. The magnetic force has no component along the magnetic field, so that it will only play a role in accelerating the wind when it is coupled with the rotation (through the centrifugal force).

The relation between dimensional parameters Ω, ϱ_*, p_*, B_{r*}, and dimensionless parameters Θ and ω is found as follows. When evaluating the constant E at the coronal base by (6), we may neglect the first two terms. By using (8) and (11c) we find

$$\tilde{E}/\omega^{1/3} = \left(\frac{\gamma}{\gamma-1}\frac{p_*}{\varrho_*} - \frac{GM}{r_*} - \frac{\Omega^2 r_*^2}{2}\right)\Big/(GM\Omega)^{2/3}. \tag{17a}$$

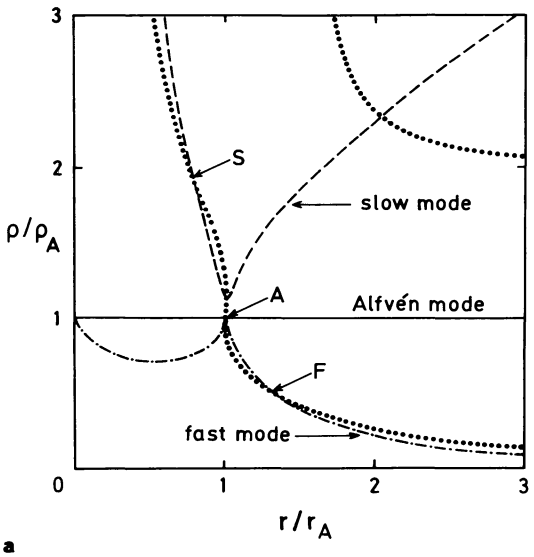

a

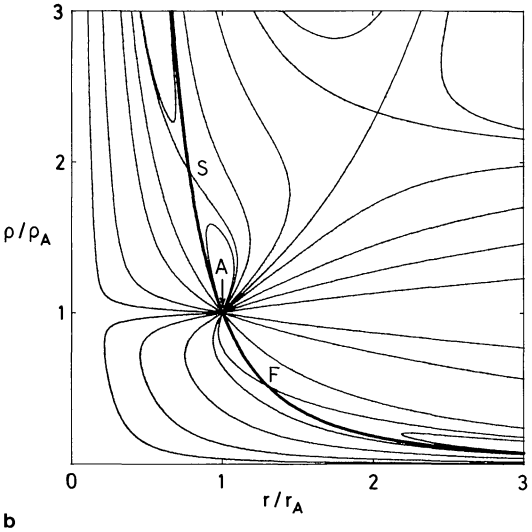

b

Fig. 1. **a** Solution plane in the Weber-Davis model. The radial flow velocity exceeds the slow, Alfvén, and fast mode velocities when the solution crosses the slow mode Mach curve (dashed), the Alfvénic line (solid), and the fast mode Mach curve (dash-dotted), respectively, from the top toward the bottom in this (r, ϱ)-plane. Dotted lines show the locus of the gravitational throat of the equivalent de Laval nozzle. The intersections of the Mach curves and the throat curves give slow mode (S) and fast mode (F) critical points. The Alfvén point is denoted by A. **b** Solution curves. The wind solution relevant to our problem is shown in a thick curve. The values of parameters ($\Theta = 0.5$, $\omega = 0.25$) are selected in such a way that the three critical points are well separated from each other

Next we will eliminate r_A and ϱ_A from (11a–c) and use $\Phi = r_*^2 B_{r*}$ to obtain

$$\beta^{\gamma-1}\Theta/\omega^{4/3-\gamma} = \frac{\gamma p_*}{\varrho_*}\left(\frac{B_{r*}^2}{4\pi\varrho_*}\right)^{\gamma-1}\Big/\left(\frac{GM}{r_*}\right)^{2\gamma-4/3}(\Omega r_*)^{2(4/3-\gamma)}. \tag{17b}$$

Two equations (17a, b) determine the values of Θ and ω in terms of dimensional parameters Ω, ϱ_*, p_*, and B_{r*}, since β and $\tilde{E}$ are known functions of Θ and ω.

One important point to be stressed is that one need not resort to the so-called "shooting method" in order to find the wind solution.

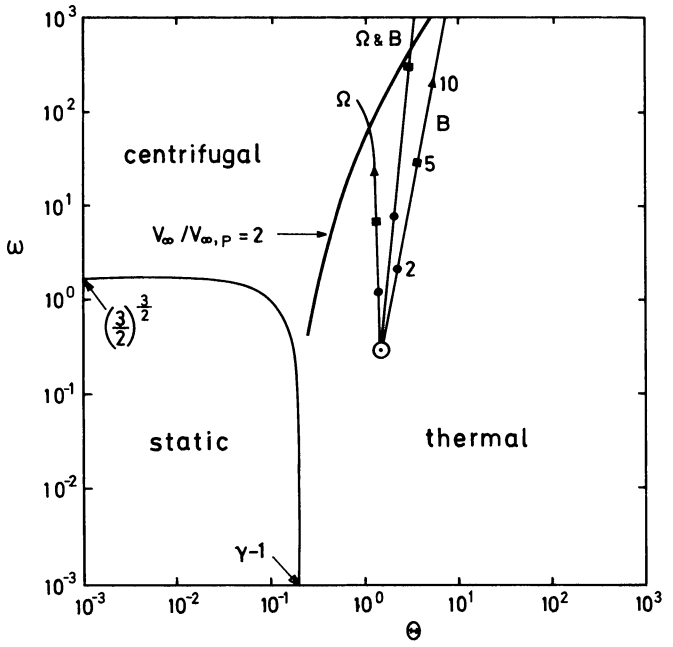

Fig. 2. Parameter space in the Weber-Davis model. The abscissa is Θ, which measures the thermal force, and the ordinate is ω, which represents the effect of the centrifugal force. No wind solution exists in the lower left part because of insufficient thermal and centrifugal forces. The lower right part is the regime of thermal winds where the centrifugal force has no essential effects. The upper left part is the regime of centrifugal winds where in turn thermal pressure is negligible. The terminal velocity of the wind, V_∞, is enhanced [compared to the case of no rotation ($V_{\infty,P}$)] toward the centrifugal wind region. The region to the left of the curve $V_\infty/V_{\infty,P}=2$ will be called the fast magnetic rotator or FMR (Belcher and MacGregor, 1976) in contrast to the other regime, the slow magnetic rotator (SMR). The solar wind model of Weber and Davis (1967) is indicated by ⊙. If the rotation rate or field strength, or both, are increased by factors 2 (indicated by circles), 5 (squares), and 10 (triangles), the model evolves along the solid curves toward the FMR regime

The simultaneous algebraic equations (16) are easily and quickly solved by the Newton-Raphson procedure, and after determining the values of x_s, x_f, y_s, y_f, $\tilde{E}$, and β, one may obtain the dimensionless density profile $y(x)$ of the wind solution by simply drawing the level contour in the (x, y)-plane. This provides a very rapid procedure to solve the wind equation, which facilitates the method of computation described in Sect. 3 for 2-*D* models.

A survey of solutions was made for a wide range of parameters Θ and ω, and the results are summarized in Fig. 2. ($\gamma=1.2$ was assumed.) No wind solutions are found in the lower left corner of the (Θ, ω)-plane, in the range of parameters roughly given by $\Theta < \gamma - 1$ and $\omega < (3/2)^{3/2}$. This is because both thermal and centrifugal forces are too weak to support the wind so that a static atmosphere comes about. The lower right region of the parameter space is the regime of thermal winds, whereas the upper left region is the regime of centrifugal winds. In the upper right region both thermal and centrifugal forces are responsible for the winds. The terminal velocity of the wind, V_∞, is essentially the same as in the case of no rotation ($V_{\infty,P}$) in the thermal wind regime. The locus of solutions with $V_\infty/V_{\infty,P}=2$ is also plotted in Fig. 2, and toward the left of this curve V_∞ is significantly enhanced compared with the Parker value $V_{\infty,P}$. This regime is called "the fast magnetic rotator (FMR)" in contrast to the case of the slow magnetic rotator (SMR, $V_\infty \simeq V_{\infty,P}$) according to Belcher and MacGregor (1976).

The solar wind model of Weber and Davis (1967) is indicated by ⊙ in Fig. 2, which has $\Theta = 1.5$ and $\omega = 0.3$. The solar wind is in the thermal wind regime. If the rotation rate or the field strength, or both, are increased, the model evolves along the curves shown in Fig. 2 toward the FMR regime. It is also in principle possible to plot the whole main sequence in this diagram, if the necessary boundary conditions (Ω, ϱ_*, p_*, and B_{r*}) are available. This was not done here because the values ϱ_*, p_*, and particularly B_{r*} are poorly known.

3. 2-D axisymmetric wind model

3.1. *Formulation of the problem*

In this section we will generalize the 1-*D* Weber-Davis model into a self-consistent 2-*D* model which satisfies the cross-field balance of force, by keeping the same basic structure of the magnetic field (i.e. the split monopole geometry). We will use spherical polar coordinates (r, θ, φ). The radius from the rotation axis $\varpi = r\sin\theta$ is also used in the following. Equations (1)–(6) are then generalized as follows. (Mestel, 1968; Okamoto, 1974). The conservation of magnetic flux is taken care of by writing

$$\boldsymbol{B} = \nabla a \times \nabla\varphi + \varpi B_\varphi \nabla\varphi\,, \tag{18}$$

where a (the magnetic stream function) and the toroidal component of the field B_φ are functions of (r, θ). The first term gives the poloidal field $\boldsymbol{B}_p$, and the poloidal field lines are represented by a family of curves $a = \text{const}$. (The azimuthal component of the usual vector potential is a/ϖ.) The velocity can be written as

$$\boldsymbol{V} = \frac{\alpha(a)}{\varrho}\boldsymbol{B} + \varpi^2\Omega(a)\nabla\varphi\,. \tag{19}$$

The first term is the velocity, parallel to the magnetic field, in the frame rotating with the angular velocity Ω. The mass conservation ($\operatorname{div}\varrho\boldsymbol{V}=0$) and the induction equation $[\nabla\times(\boldsymbol{V}\times\boldsymbol{B})=0]$ are satisfied if the two scalars α and Ω are functions of a. The dependence of Ω on a allows the differential rotation of the star in the model. It is straightforward to generalize (1), (5), and (6), i.e.

$$p = K(a)\,\varrho^\gamma, \tag{20}$$

$$\varpi\left(V_\varphi - \frac{B_\varphi}{4\pi a}\right) = \Omega\varpi_A^2(a)\,, \tag{21}$$

$$\frac{V_p^2}{2} + \frac{1}{2}(V_\varphi - \Omega\varpi)^2 + \frac{\gamma}{\gamma-1}\frac{p}{\varrho} - \frac{GM}{r} - \frac{\Omega^2\varpi^2}{2} = E(a)\,, \tag{22}$$

where $\boldsymbol{V}_p = \alpha\boldsymbol{B}_p/\varrho$ is the poloidal velocity and $\varpi_A(a)$ is the Alfvén radius. Insteas of six constants K, f, Φ, Ω, r_A, and E in Sect. 2, we have introduced five "field-line constants" $K(a)$, $\alpha(a)$, $\Omega(a)$, $\varpi_A(a)$, $E(a)$, and a stream function a.

If the function a is given, these Eqs. (18)–(22) describe the wind along each field line $a = \text{const}$. Given the rotation rate Ω, the boundary conditions on the density and the pressure at the base of the corona together with the conditions at the slow/fast mode critical points uniquely determine the constants $K(a)$, $\alpha(a)$, $\varpi_A(a)$, and $E(a)$, and consequently, the density profile, as in Sect. 2. The Bernoulli equation for this purpose is

$$\frac{\alpha^2}{2\varrho^2}\left(\frac{\nabla a}{\varpi}\right)^2 + \frac{1}{2}\left[\frac{4\pi\alpha^2\Omega(\varpi_A^2-\varpi^2)}{\varpi(4\pi\alpha^2-\varrho)}\right]^2 + \frac{\gamma K}{\gamma-1}\varrho^{\gamma-1} - \frac{GM}{r} - \frac{\Omega^2\varpi^2}{2} = E\,. \tag{23}$$

Therefore the remaining process is to determine a by the the equation of force-balance across the field lines. After some manipulation we can rewrite the equation of motion as (Okamoto, 1975; Heinemann and Olbert, 1978)

$$0 = -\nabla p + \frac{1}{4\pi}(\nabla \times \boldsymbol{B}) \times \boldsymbol{B} + \varrho \nabla \frac{GM}{r} - \varrho(\boldsymbol{\varpi} \cdot \nabla)\boldsymbol{\varpi}$$
$$= \nabla a \left\{ \mathrm{div}\left[\left(\frac{a^2}{\varrho} - \frac{1}{4\pi}\right)\frac{\nabla a}{\varpi^2}\right] - \varrho\left(E' - \frac{1}{\gamma - 1}\frac{p}{\varrho}\frac{K'}{K} + \varpi^2 \Omega \Omega'\right) - \frac{B^2}{\varrho}\alpha\alpha' - \varpi B_\varphi\left[(\alpha\Omega)' - \frac{1}{\varpi^2}(\alpha\Omega\varpi_A^2)'\right]\right\}, \quad (24)$$

where prime (′) denotes d/da. Since the force-balance in the φ-direction and along the magnetic field is already taken care of by (21) and (22), Eq. (24) has only the cross-field component in the direction ∇a. Therefore the equation to be solved is

$$\mathrm{div}\left[\left(\frac{\alpha^2}{\varrho} - \frac{1}{4\pi}\right)\frac{\nabla a}{\varpi^2}\right] = \varrho\left(E' - \frac{1}{\gamma - 1}\frac{p}{\varrho}\frac{K'}{K} + \varpi^2 \Omega \Omega'\right) + \frac{B_p^2}{\varrho}\alpha\alpha' + D\left[\frac{D}{4\pi}\Omega^2\varpi^2\alpha\alpha' - \alpha^2\Omega^2\varpi_A^2{}' - \alpha^2\Omega\Omega'(\varpi_A^2 - \varpi^2)\right],$$
$$D = \frac{4\pi\varrho(\varpi_A^2 - \varpi^2)}{\varpi^2(4\pi\alpha^2 - \varrho)}, \quad (25)$$

where ϱ is an implicit function of r, θ, a, and ∇a via (23).

Equation (25) is a second-order quasi-linear partial differential equation for a, with the second-order derivatives of a in the left-hand side. A fundamental property of this equation becomes transparent if we pick up its principal term. That is,

$$\mathrm{div}\left\{\left(\frac{\alpha^2}{\varrho} - \frac{1}{4\pi}\right)\frac{\nabla a}{\varpi^2}\right\} = -\frac{\alpha^2}{\varrho^2}\nabla\varrho \cdot \frac{\nabla a}{\varpi^2} + \frac{1}{\varpi^2}\left(\frac{\alpha^2}{\varrho} - \frac{1}{4\pi}\right)\nabla^2 a + (\text{lower-order terms}). \quad (26)$$

The differentiation of (23) yields

$$\frac{\alpha^2}{2\varpi^2}\nabla(\nabla a)^2 - \frac{V_p^4 - V_p^2(C_s^2 + V_{Ap}^2 + V_{A\varphi}^2) + C_s^2 V_{Ap}^2}{V_p^2 - V_{Ap}^2}\nabla\varrho + (\text{lower-order terms}) = 0, \quad (27)$$

where $V_{Ap}^2 = B_p^2/4\pi\varrho$, $V_{A\varphi}^2 = B_\varphi^2/4\pi\varrho$. Therefore (25) can be written as

$$\frac{1}{4\pi\varpi^2}\left(\frac{V_p^2}{V_{Ap}^2} - 1\right)\cdot\left[\nabla^2 a - \frac{\nabla\nabla a : \nabla a \nabla a}{(\nabla a)^2}\frac{V_p^4}{V_p^4 - V_p^2(C_S^2 + V_{Ap}^2 + V_{A\varphi}^2) + C_S^2 V_{Ap}^2}\right] = g(r, \theta, a, \nabla a), \quad (28)$$

with the dyadic notation

$$\nabla\nabla a : \nabla a \nabla a = \sum_{i,j=1}^{3} \frac{\partial^2 a}{\partial x_i \partial x_j}\frac{\partial a}{\partial x_i}\frac{\partial a}{\partial x_j} \quad (29)$$

and the explicit form of g is easily obtained from (25). The important character of the equation is that the coefficient of the second order derivatives vanishes if $\varrho = 4\pi\alpha^2$, or equivalently, if $V_p = V_{Ap}$. The equation is singular at the Alfvén point. We will select a solution regular at the Alfvén singularity as follows. First (28) itself requires $g = 0$ at the Alfvén point. Therefore the second derivatives there can be finite but are represented as zero divided by zero. A definite expression for the second derivatives is however obtained by applying the l'Hopital's rule to (28). That is, by differentiating (28) with respect to r at the Alfvén point A, we obtain

$$\left[\nabla^2 a - \frac{\nabla\nabla a : \nabla a \nabla a}{(\nabla a)^2}\frac{V_p^4}{V_p^4 - V_p^2(C_S^2 + V_{Ap}^2 + V_{A\varphi}^2) + C_S^2 V_{Ap}^2}\right]_A = 4\pi\varpi_A^2\left[\frac{\partial g}{\partial r}\right]_A \Big/ \left[\frac{\partial}{\partial r}\left(\frac{V_p^2}{V_{Ap}^2} - 1\right)\right]_A. \quad (30)$$

Consequently, two equations must be satisfied at the Alfvén point, and (30) based on l'Hopital's rule is regarded as the boundary condition. Therefore two boundary conditions are imposed on a, one at the coronal base where a is specified, and the other at the Alfvén point by l'Hopital's rule. The regularity condition at the Alfvén point is equivalent to eliminating the standing Alfvén shock. Without the regularity requirement, the field lines may have a "kink" at the Alfvén point. These two conditions are sufficient to determine a, and in particular it is not necessary to assume any boundary conditions at infinity.

Another important character of (28) is that it is of mixed type, i.e. it is elliptic in some part of the volume and is hyperbolic in the rest. To see this we will replace $\nabla^2 a$ and $\nabla\nabla a$ by $-k^2 a$ and $-\boldsymbol{kka}$ in the principal term of (28). The wave vector $\boldsymbol{k}$ is found as

$$\frac{k_\parallel^2}{k_\perp^2} = \frac{V_p^2(C_S^2 + V_{Ap}^2 + V_{A\varphi}^2) - C_S^2 V_{Ap}^2}{V_p^4 - V_p^2(C_S^2 + V_{Ap}^2 + V_{A\varphi}^2) + C_S^2 V_{Ap}^2} = \frac{(V_p^2 - V_{cp}^2)(C_S^2 + V_{Ap}^2 + V_{A\varphi}^2)}{(V_p^2 - V_{sp}^2)(V_p^2 - V_{fp}^2)}, \quad (31)$$

where $k_\parallel$ and $k_\perp$ refer to the components of $\boldsymbol{k}$ parallel and perpendicular to the poloidal magnetic field $\boldsymbol{B}_\mathrm{p}$, and

$$V_{cp}^2 = \frac{C_S^2 V_{Ap}^2}{C_S^2 + V_{Ap}^2 + V_{A\varphi}^2}. \quad (32)$$

If the right-hand side of (31) is positive (negative), $\boldsymbol{k}$ is real (imaginary) and the equation is hyperbolic (elliptic), respectively. Namely the equation is elliptic if $V_p < V_{cp}$ or $V_{sp} < V_p < V_{fp}$ and is hyperbolic if $V_{cp} < V_p < V_{sp}$ or $V_{fp} < V_p$ (Heinemann and Olbert, 1978). [V_{sp} and V_{fp} are poloidal components of slow/fast mode wave velocities, defined similarly as in (13).] The fact that the equation for a does not require a boundary condition at infinity is now understood, because the flow far from the star is faster than the fast mode speed so that no MHD signal can propagate upstream and the solution there is completely determined by the condition within the fast mode critical point.

3.2. *Computational procedure*

Equation (25) will be solved in the region $r_\mathrm{in} \leqq r \leqq r_\mathrm{out}$ and $0 \leqq \theta \leqq \pi/2$. (Equatorial symmetry is assumed.) The inner boundary r_in is chosen to be sufficiently smaller than the smallest value of r_s (slow mode critical radius) over the field lines in $0 \leqq \theta \leqq \pi/2$. We will impose the boundary condition $B_r = \mathrm{const}$ (i.e. a monopole field) at $r = r_\mathrm{in}$. The outer boundary r_out is taken to be slightly larger than the largest value of r_f (fast mode critical radius). As was described previously, the outer boundary condition on a is given at the Alfvén radius so that (25) might look solvable even in the region $r_\mathrm{in} \leqq r \leqq r_A$ *if the density profile is known*. As a matter of fact the density profile depends, among others, on the location of the fast

mode critical points. Therefore the volume $r_{in} \leqq r \leqq r_{out}$ must be solved simultaneously. On the other hand the solution outside the radius r_{out} can simply be obtained by integrating (25) outward, since (25) is hyperbolic there and the value of a itself and its derivative are given at $r = r_{out}$ through the solution found in $r_{in} \leqq r \leqq r_{out}$.

The monopole field ($B_r = \Phi/r^2$) is represented by $a = 2\Phi \sin^2(\theta/2)$. Therefore it is useful to introduce a variable θ_0 instead of a by the relation $a(\theta_0) = 2\Phi \sin^2(\theta_0/2)$. And for computational convenience we will change the independent variables from (r, θ) to (r, θ_0) and will look for the solution $\theta = \theta(r, \theta_0)$. The left-hand side of (25) is now expressed as

$$\mathrm{div}\left[\left(\frac{\alpha^2}{\varrho} - \frac{1}{4\pi}\right)\frac{\nabla a}{\varpi^2}\right] = -\frac{\Phi}{r^2}\left[\frac{\partial}{\partial r} - \frac{\partial\theta}{\partial r}\left(\frac{\partial\theta}{\partial\theta_0}\right)^{-1}\frac{\partial}{\partial\theta_0}\right]\left[\left(\frac{\alpha^2}{\varrho} - \frac{1}{4\pi}\right)\frac{\sin\theta_0}{\sin^2\theta}\left(\frac{\partial\theta}{\partial\theta_0}\right)^{-1}\frac{\partial\theta}{\partial r}\right] + \frac{\Phi}{r\sin\theta}\left(\frac{\partial\theta}{\partial\theta_0}\right)^{-1}\frac{\partial}{\partial\theta_0}\left[\left(\frac{\alpha^2}{\varrho} - \frac{1}{4\pi}\right)\frac{\sin\theta_0}{r}\left(\frac{\partial\theta}{\partial\theta_0}\right)^{-1}\frac{1}{r^2\sin\theta}\right], \tag{33}$$

and in the left-hand side of (25), $d/da = (\Phi \sin\theta_0)^{-1} d/d\theta_0$, and B_p^2 is given by

$$B_p^2 = \left(\frac{\nabla a}{\varpi}\right)^2 = \left(\frac{\Phi\sin\theta_0}{r\sin\theta}\right)^2\left(\frac{\partial\theta}{\partial\theta_0}\right)^{-2}\left[\frac{1}{r^2} + \left(\frac{\partial\theta}{\partial r}\right)^2\right]. \tag{34}$$

Equation (25) is then solved numerically by dividing the (r, θ_0)-space into a finite-sized grid. Since field lines are labelled by θ_0, the method used here is Lagrangian across the field (the grid moving together with the field lines), and is Eulerian in the r-direction. The grid in the r-direction is not fixed, however, but is flexible in such a way that, for each field line, one grid point is always located exactly at the Alfvén point. This is necessary to handle the singularity at the Alfvén point properly. In the examples shown below, we used 10 grid points in θ_0 (10° spacing) and 15–20 grid points in r, nearly equally spaced in $\log r$. The boundary condition at $r = r_{in}$ is simply written as $\theta = \theta_0$, and of course $\theta = 0$ at $\theta_0 = 0$ and $\theta = \pi/2$ at $\theta_0 = \pi/2$.

We take $\gamma = 1.2$ as in the 1-*D* model described in Sect. 2. We assume that $\Omega(\theta_0)$ is a constant given by the angular velocity of the (rigidly rotating) star. We will also assume that $K(\theta_0)$ and $E(\theta_0)$ are constants, being independent of θ_0. This assumption is justified if the star rotates slowly so that the atmosphere near the stellar surface is almost static and spherically symmetric. For fast rotators this assumption may be violated. The parameters $\alpha(a)$ and $\omega_A(a)$ are to be determined self-consistently at each iteration stage, by requiring that the density profile passes through slow and fast critical points. (The location of the critical points is also updated in each iteration.)

Before solving (25), we first determine the Weber-Davis model for the same parameter setting. The Alfvén radius r_A and the Alfvén density ϱ_A are thus obtained, which will be designated here as $r_{A,WD}$ and $\varrho_{A,WD}$ respectively in order to make it explicit that these values are for the Weber-Davis model. Then (25) will be solved in the dimensionless form in which $r_{A,WD}$ and $\varrho_{A,WD}$ are used as the length and the density units, respectively.

As in Sect. 2, the model is specified by two dimensionless parameters Θ and ω,

$$\Theta = \frac{\gamma K \varrho_{A,WD}^{\gamma-1} r_{A,WD}}{GM}, \tag{35a}$$

$$\omega = \frac{\omega^2 r_{A,WD}^3}{GM}. \tag{35b}$$

Solutions were looked for in the part of parameter space (Fig. 2) where r_s, r_A, and r_f are of the same order and the computation is easiest, namely, $\Theta, \omega \simeq 1$. The discretized version of (25) was solved iteratively by the Newton-Raphson procedure. The initial guess for the solution can be the radial field if ω is small. Once the solution is obtained, it is used as the initial guess for the next solution with a larger value of ω.

3.3. *Computational results*

Figures 3–6 show an example calculated for $\Theta = 0.5$ and $\omega = 1.75$. First we will discuss the behavior of the solution in the region $r \leqq r_{out}$ ($r_{out} = 4r_{A,WD}$ in the example shown below). Figure 3a shows the location of three (slow, Alfvén, fast) critical surfaces in the poloidal plane before the iteration (i.e. for the fixed radial magnetic field). Figure 3b is the self-consistent solution after the iteration was carried out. The poloidal field lines are deflected toward the pole significantly as compared to the original radial field. This is mainly due to the build-up of the toroidal magnetic field (see Fig. 4). Since the field lines are more tightly wound near the equator while $B_\varphi = 0$ on the rotation axis, B_φ^2 is larger near the equator and is smaller near the pole and the gradient in the magnetic pressure $-\nabla B_\varphi^2/8\pi$ is directed away from the equator. This effect was first noticed by Suess (1972), Winge and Coleman (1974) and by Nerney and Suess (1975) in the case of the solar wind. In addition the magnetic tension due to B_φ is also directed toward the pole. Because of this poleward deflection of the field lines, the cross section of the flow channel near the rotation axis becomes smaller than the radial ($\sim r^2$) opening. Therefore the efficiency in accelerating the wind is decreased, the transition to the supersonic velocity is postponed to larger distances, and the critical surfaces are pushed outward consequently. On the other hand near the equator a wider opening of the flow channel gives a more efficient acceleration and the critical surfaces are displaced inward. The mass flux per unit magnetic flux [i.e. α in Eq. (19)] is also enhanced near the equator. The terminal velocity of the wind V_∞ is found as $V_\infty^2/2 = E + \Omega^2 \varpi_A^2/2$ from the Bernoulli equation (23) [see Eq. (37)]. Therefore if the wind model is in the SMR regime, the flow velocity quickly (slowly) reaches the same terminal velocity $V_\infty \simeq \sqrt{2E}$ near the equator (the pole) respectively, because of the flow geometry described above. For FMR's of course the terminal velocity is significantly enhanced near the equator.

Figure 4 shows the structure of magnetic field lines and stream lines in the equatorial plane. Circles represent slow, Alfvén, and fast mode critical surfaces, respectively, from inside to outside. The field lines exhibit a spiral pattern showing the build-up of the toroidal magnetic field. The stream lines show that the flow is nearly ballistic far from the star. It is also seen that the flow carries the angular momentum because the outer, straight part of the stream lines, if extended inward, does not go through the origin. Figure 5 depicts the out-of-equator structure of magnetic field lines projected onto the meridional plane. The winding of field lines becomes increasingly tight near the rotation axis as well.

3.4. *Asymptotic behavior of the solution at large distances*

Next we will study the behavior of the solution at large distances from the star. The outward integration of (25) in the hyperbolic region $r > r_{out}$ revealed that the deflection of the field lines toward the rotation axis becomes slower and slower but continues

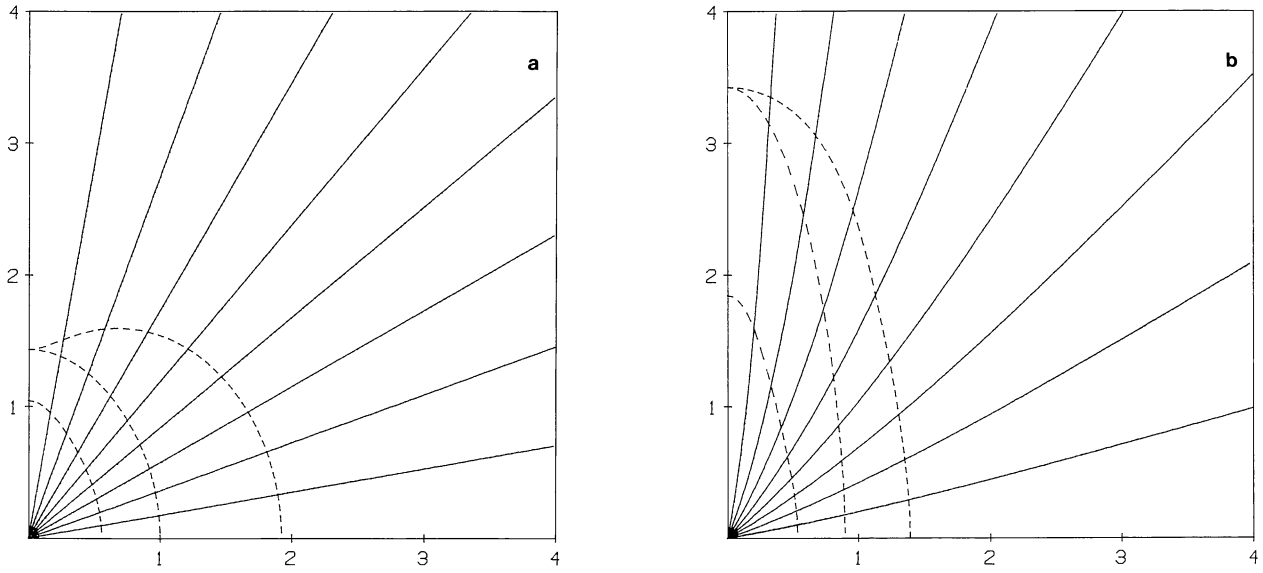

Fig. 3. **a** Location of slow, Alfvén, and fast mode critical surfaces (from inside to outside, respectively) in the poloidal plane when the magnetic field is radial. The unit of length is $r_{A,WD}$. **b** Self-consistent configuration of the magnetic field. Field lines are bent toward the pole, and the critical surfaces are displaced outward (inward) near the pole (equator), respectively, compared to **a**

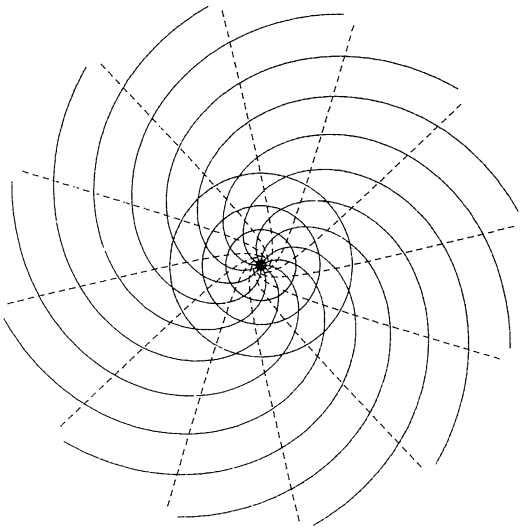

Fig. 4. Magnetic field lines (solid) and flow stream lines (dashed) in the equatorial plane ($0 \leqq r \leqq 4r_{A,WD}$). Three circles represent the location of the three critical surfaces shown in Fig. 3b

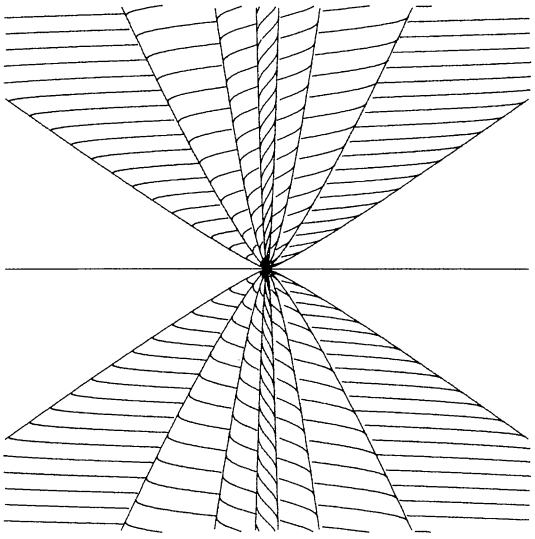

Fig. 5. Meridional view of the spiraling field lines ($0 \leqq r \leqq 50 r_{A,WD}$). The horizontal line indicates the equatorial plane. Field lines are on the nested cones that represent the magnetic surfaces $\theta_0 = \text{const}$ ($=10°$, $30°$, $50°$, $70°$). In this figure are drawn only those parts of the field lines which run away from us on the left-hand side of the picture, pass behind the polar axis, and then return toward us on the right. The other parts, which are in front of the plane of the paper, are omitted to avoid overlapping. A part of the magnetic surfaces which is behind other magnetic surfaces is also suppressed

indefinitely. Figure 6 shows the structure of the solution in the polar coordinates $(\log r, \theta)$, instead of the usual (r, θ), in order to cover the wide range in r. (Near the rotation axis θ decreases roughly as $\theta \sim 1/r$ so that $\varpi \sim$ constant. The apparent convergence toward the axis is because of the logarithmic scaling in r.) There is no indication that the solution approaches to the radial configuration ($\theta \to$ const).

This behavior of the solution can be studied semi-analytically as follows. The numerical solution indicates that, for large values of r, the behavior of the solution is described by dividing the θ_0-space into three regions. In the inner (polar) region $0 \leqq \theta_0 \leqq \theta_{0a}$, both the tension and the pressure forces due to B_φ are directed poleward and are counterbalanced by the gas pressure. In the intermediate region $\theta_{0a} \leqq \theta_0 \leqq \theta_{0b}$, the tension and the pressure forces of B_φ are balanced by themselves, and the effect of gas pressure is negligible. And in the outer (equatorial) region $\theta_{0b} \leqq \theta_0 \leqq \pi/2$, the poleward force due to B_φ is compensated by the inertia of the flow $\varrho(\boldsymbol{V} \cdot \nabla)\boldsymbol{V}$ (in other words the flow is deflected by the

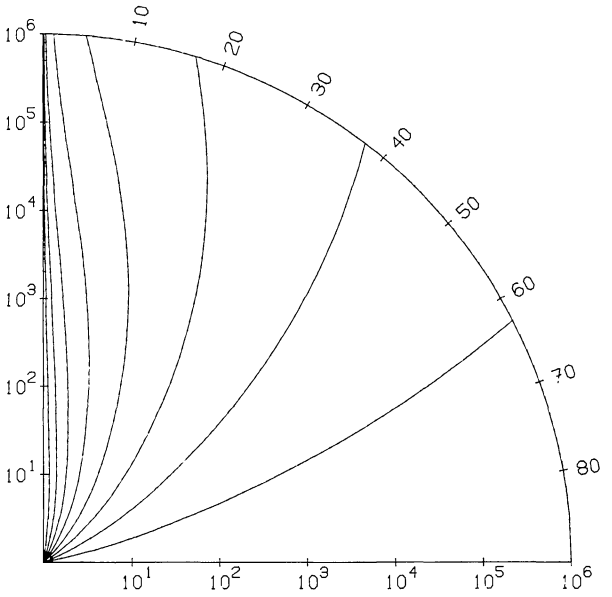

Fig. 6. The structure of the poloidal field at large distances, plotted in logarithmic scale in r. The flow is continuously deflected toward the rotation axis. At $r = 10^6 r_{A,WD}$, the field lines with $\theta_0 \leqq 50°$ are bundled into a cone $\theta \leqq 5°$

magnetic force). In the inner and the intermediate regions $\partial\theta/\partial r$ is negligible so that the equation to be solved reduces to an ordinary differential equation which only involves $\partial/\partial\theta_0$. In the outer region we can assume a separable form $\theta \simeq \pi/2 + f(r)(\theta_0 - \pi/2)$. The approximate solutions in the three regions are then connected at θ_{0a} and θ_{0b} to give an asymptotic solution valid for the whole range in θ_0.

The "cut and paste" procedure described above leads to the following results. The angle θ_{0a} scales as $\theta_{0a} \sim (\log r)^{-1/2} \ll 1$. In the polar region $0 \leqq \theta_0 \leqq \theta_{0a}$ the density decays very slowly in r, i.e. $\varrho \sim (\log r)^{-1/(\gamma-1)}$, and the pressure of this dense gas balances the pinching force due to B_φ. The radius of this inner region increases only logarithmically, that is, the flow is almost cylindrical. The effect of the poloidal magnetic pressure is negligible compared to the gas pressure, because $p \sim (\log r)^{-\gamma/(\gamma-1)}$ while $B_p^2 \sim (\log r)^{-2/(\gamma-1)}$. This dense polar column is a typical pinch configuration and could be unstable due to sausage/kink instabilities. In the very central part of this column, however, $B_p^2 > B_\varphi^2$ holds so that the stabilizing effect of B_p might be important. The angle θ_{0b} is close to $\pi/2$, i.e. $\pi/2 - \theta_{0b} \sim (\log r)^{-1} \ll 1$. In the intermediate and outer regions $\theta_{0a} \leqq \theta_0 \leqq \pi/2$, θ behaves like $\theta \sim r^{-\nu}$, where the exponent $\nu(\theta_0)$ varies from $\simeq 1$ near the rotation axis to $\simeq 0$ near the equator. The asymptotic form $\theta \sim r^{-\nu}$ means that, if r is very large, θ is almost zero everywhere except in the very vicinity of $\theta_0 = \pi/2$ (equator). That is, almost all the field lines are deflected toward the direction of the rotation axis. The density decays as $\varrho \sim r^{-2+2\nu}/\log r$. Therefore the density at the equator is much less than that on the rotation axis.

The asymptotic behavior of the solution described above is a natural consequence of the build-up of B_φ. Therefore, however small Ω is, the wind will finally be collimated. The wind model with $\Omega = 0$ ($B_\varphi = 0$), in which the flow will become radial far from the star, is qualitatively different from our model. Further, from the Bernoulli equation (22) we find that the terminal velocity V_∞ is given by

$$\frac{V_\infty^2}{2} = E + \Omega^2 \varpi_A^2 \left[1 - \frac{(\varrho\varpi^2)_\infty}{(\varrho\varpi^2)_A}\right]. \tag{36}$$

If the solution approaches to a radial configuration at infinity, $(\varrho\varpi^2)_\infty$ converges to a finite value (this is also the case for the 1-D Weber-Davis model). In our asymptotic solution we found $\varrho\varpi^2 \sim 1/\log r \to 0$, therefore,

$$\frac{V_\infty^2}{2} = E + \Omega^2 \varpi_A^2. \tag{37}$$

The same ratio $R = (\varrho\varpi^2)_\infty/(\varrho\varpi^2)_A$ appears also in the ratio between energy densities at infinity, $\frac{1}{2}\varrho V^2 : B^2/8\pi = E + \Omega^2\varpi_A^2 (1-R) : \Omega^2 \varpi_A^2 R$. The angular momentum decrease of the star is due to the sum of the angular momentum carried away by the flow and the magnetic braking torque. The ratio between the two is $1-R : R$. Although $R \simeq 3/4$ in the solar wind model of Weber and Davis (1967), our analysis shows that the magnetic torque plays less and less a role ($R \to 0$ as $r \to \infty$) in braking the rotation of the star.

4. Summary and discussion

In this paper we have developed a method to calculate steady, axisymmetric wind models with frozen-in magnetic fields, as a straightforward extention of the one-dimensional Weber-Davis model. The wind solution along the magnetic field is given by an algebraic equation (the Bernoulli equation) for the density. There appear two critical points, the slow mode and the fast mode critical points. The shape of the magnetic field should be determined in such a way that the force-balance across the field is satisfied. This leads to a second order partial differential equation for the magnetic stream function a and two boundary conditions are necessary to determine the solution. One condition is given at the inner boundary (i.e. the coronal base) where a is specified, and the other condition is supplied at the Alfvén surface where the coefficients of the second order derivatives of a vanish. In order to have well-behaved second order derivatives of a there, l'Hopital's rule is applied and gives the constraint. A numerical scheme was developed following this basic formulation, and an example of solution was presented in Sect. 3. The basic feature of the solution is the poleward deflection of the flow due to the build-up of toroidal magnetic field in the wind. The asymptotic behavior of the solution at large distances shows that almost all the field lines are deflected toward the direction of the rotation axis, i.e., the flow becomes collimated. The wind is almost cylindrical near the rotation axis, and there arises a polar column in which high gas density is produced by the pinching effect of the toroidal magnetic field.

If we compare our method with that of Pneuman and Kopp (1971), the apparent lack of the Alfvén singularity in their treatment is striking. Our Eq. (28) can be written in the form

$$\nabla^2 a = \frac{V_p^2}{V_{Ap}^2}\nabla^2 a + \frac{\nabla\nabla a : \nabla a \nabla a}{(\nabla a)^2} \frac{V_p^2 (V_p^2/V_{Ap}^2 - 1)}{V_p^4 - V_p^2 (C_S^2 + V_{Ap}^2 + V_{A\varphi}^2) + C_S^2 V_{Ap}^2} + 4\pi\varpi^2 g. \tag{38}$$

Their iterative procedure is to evaluate the right hand side of (38) for the n-th iterate a_n and to calculate the $(n+1)$-th iterate a_{n+1} by solving (38) as the Poisson equation. Thus the singularity at $V_p = V_{Ap}$ is apparently lost because the term $(1 - V_p^2/V_{Ap}^2)\nabla^2 a$ was split into two: $\nabla^2 a_{n+1}$ on the left hand side and $V_p^2/V_{Ap}^2 \nabla^2 a_n$ on the right hand side as the source term. Instead of losing the regularity condition at the singularity, they imposed the additional

boundary condition that the field lines become radial at infinity. A question that could be asked is then whether the difference between their and our methods is only a methodological one or not. As was pointed out by Okamoto (1975) and also is clear from the argument given in Sect. 3, their formulation of the problem has no explicit condition to exclude singular solutions and therefore a unique regular solution may not be obtained by their method. The solution they gave, however, looks smooth at the Alfvén point. It could be possible that the solution of their iterative procedure may depend on the initial guess and, by starting from a smooth initial state, the iteration may converge toward a smooth solution. In any case their method is not applicable if $\Omega \neq 0$, because the solution does not become radial at infinity.

Our method has some mathematical uncertainty, too. Firstly, the equation was solved in the volume $r_{\rm in} \leqq r \leqq r_{\rm out}$ as a boundary value problem. The existence of hyperbolic regions in the volume practically caused no problem so far, but there might be a more rigorous treatment for them. Secondly, since the outer boundary condition is given at r_A, our method might be regarded as solving the Cauchy problem in the elliptic region $r_A < r < r_f$. As is well known, this is an ill-posed problem and the method will be unstable. Physically the instability may develop as follows. Suppose the mass flux [or $\alpha(a)$ of Eq. (19)] is kept constant. Then if the two neighboring field lines are perturbed and come closer to each other in the region $r_A \leqq r \leqq r_f$, the flow velocity between the two field lines increases and the density there decreases. The pressure force therefore makes the field lines converge further and the instability will grow. However in the actual computation this behavior is never found because $\alpha(a)$ is not fixed but changes in response to the variation of the field geometry. What actually happens in the above process is that, if the flux tube is compressed, the acceleration is suppressed because of a narrowed flow channel and the density increases instead. We might say that the type of equations (elliptic or hyperbolic) is a local character and will not fully describe the non-local feedback mentioned above. On the other hand when we tried to solve (25) for a fixed density profile [fixed $\alpha(a)$], the scheme was unstable in the elliptic region $r_A < r < r_f$. Therefore the wind equation along the field and the force-balance equation across the field should be solved simultaneously and cannot be solved alternatively.

Finally, let us consider the wind due to an oblique rotator as a simple application of our model. Of course the monopole has no magnetic axis, but the philosophy of the split monopole model is that any magnetic surface can be a current sheet separating positive and negative magnetic regions. Figure 7 depicts the structure of the magnetic surface which is tilted 10° with respect to the equator near the star, showing the "ballerina skirt" behavior. Needless to say, the oblique rotator generally needs a 3-*D* modelling.

The next step in improving our model is to include the dead zone in order to construct a more realistic model. Another interesting possibility is the application of the present method to accretion disks permeated by magnetic fields. Although self-similar solutions for this problem have been worked out e.g. by Blandford and Payne (1982), our present method makes it possible to explore solutions in much wider variety. These projects will be carried out in the following papers.

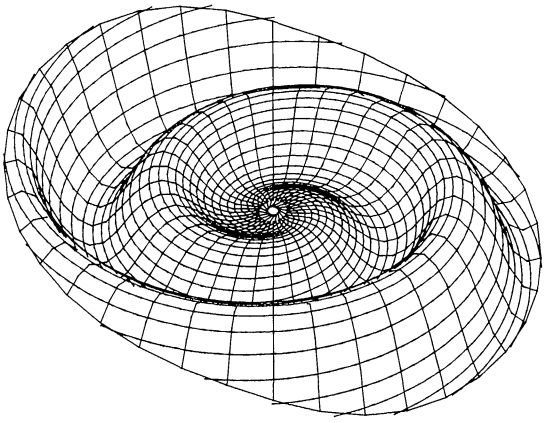

Fig. 7. The structure of the current sheet expected for an oblique rotator. The field lines constituting the magnetic surface, which can be regarded as the current sheet in the split monopole model, are selected from the model shown in Figs. 3–6

Acknowledgements. The author would like to thank Dr. H.C. Spruit for many illuminating discussions, and also Drs. U. Anzer, F. Meyer, and H.U. Schmidt for a careful reading of the manuscript. He is grateful to Prof. R. Kippenhahn for the warm hospitality during his stay at the Max-Planck-Institut für Astrophysik. Computations were carried out on the CRAY-1 of the Computer Center of the Max-Planck-Institut in Garching.

References

Belcher, J.W., MacGregor, K.B.: 1976, *Astrophys. J.* **210**, 498
Blandford, R.D., Payne, D.G.: 1982, *Monthly Notices Roy. Astron. Soc.* **199**, 883
Heinemann, M., Olbert, S.: 1978, *J. Geophys. Res.* **83**, 2457
Mestel, L.: 1961, *Monthly Notices Roy. Astron. Soc.* **122**, 473
Mestel, L.: 1967, in *Plasma Astrophysics*, ed. P.A. Sturrock, Academic Press, New York, p. 185
Mestel, L.: 1968, *Monthly Notices Roy. Astron. Soc.* **138**, 359
Nerney, S.F., Suess, S.T.: 1975, *Astrophys. J.* **196**, 837
Okamoto, I.: 1974, *Monthly Notices Roy. Astron. Soc.* **166**, 683
Okamoto, I.: 1975, *Monthly Notices Roy. Astron. Soc.* **173**, 357
Parker, E.N.: 1958, *Astrophys. J.* **128**, 664
Parker, E.N.: 1963, Interplanetary Dynamical Processes, Interscience, p. 51
Pneuman,G.W., Kopp, R.A.: 1971, *Solar Phys.* **18**, 258
Schatzman, E.: 1962, *Ann. Astrophys.* **25**, 18
Suess, S.T.: 1972, *J. Geophys. Res.* **77**, 567
Weber, E.J., Davis, L., Jr.: 1967, *Astrophys. J.* **148**, 217
Winge, C.R., Jr., Coleman, P.J., Jr.: 1974, *Planetary Space Sci.* **22**, 439
Yeh, T.: 1976, *Astrophys. J.* **206**, 768